CONCURRENT CLUTTER AND NOISE SUPPRESSION VIA LOW RANK PLUS SPARSE OPTIMIZATION FOR NON-CONTRAST ULTRASOUND FLOW DOPPLER PROCESSING IN MICROVASCULATURE

Mahdi Bayat and Mostafa Fatemi
Department of Biomedical Engineering and Physiology
Mayo Clinic College of Medicine and Science
Rochester, MN, USA
{bayat.mahdi, fatemi.mostafa}@mayo.edu

ABSTRACT

A low rank plus sparse framework for concurrent clutter and noise suppression in Doppler processing of echo ensembles obtained by non-contrast ultrasound imaging is presented. A low rank component which represents mostly strong tissue clutter signal and a sparse component which represents mostly blood echoes received from slow flows in microvasculature are assumed. The proposed method is applied to simulated data and its superior performance over conventional singular value thresholding in removing clutter and background noise is presented.

Index Terms— Low rank plus sparse, ultrasound Doppler, microvasculature, slow flow, tissue motion

1. INTRODUCTION

Detection of small Doppler shifts resulting from motion of the red blood cells in small vessels is a challenging task in medical ultrasound. Often times, tissue motions due to physiological activities (e.g. respiration or blood pulsation) or sonographer's hand motions create Doppler shifts which can speared into the frequency spectrum of the weak Doppler shifts of interest, hence causing classic wall filters to fail. Therefore, the use of ultrasound Doppler has been mainly limited to large scale hemodynamics in large vessels. Despite the Fourier spectral overlap, echo variations due to tissue motions are mostly low rank. This stems from the continuity of tissue displacements which prohibits arbitrary motions. Recently, singular value thresholding (SVT) of high frame rate ultrasound echoes has shown to provide significant advantages over classic infinite impulse response (IIR) wall filters enabling visualization of the microvasculature with unprecedented clarity[1-3]. While SVT filtering had been previously studied for clutter removal in larger vessels and hemodynamic analysis [4-7], long Doppler ensembles combined with plane wave imaging are believed to be the key in successful clutter removal for microvasculature imaging and slow flow analysis. The latter provides spatial coherence via acquiring Doppler ensemble from the entire field of view at one shot and the former provides strong temporal coherence. The two components together create a suitable framework for clutter removal via low rank SVT. However, as shown in this paper, SVD presents two main limitations. One is related to the complex tissue motions that can create strong eigen spectral overlap between tissue echoes and those from slow flows and the other is related to the additive measurement noise which covers the entire frequency and eigen spectral domains. The method in [2] provides an empirical approach for selection of the maximum rank due to tissue motion for clutter removal. However, this selection was mainly based on the frequency analysis of the singular vectors themselves which might still present tissue motion components. Additionally, a noise suppression method based on SVD truncation was proposed in [2] which was based on the decay rate of the singular values of random matrices [8]. However, the study in [9] showed that in more realistic scenarios where tissue (and hence the embedded vessels) undergo both translational and shearing motions, no differentiating rank decay can be observed between the noise and blood components. Here, we introduce a new framework for concurrent clutter removal and noise suppression. The proposed method is based on a low rank plus sparse optimization which models tissue echoes as a low rank sub-space and enforces sparsity on the blood Doppler representation in the spatial and frequency domains. Addition of the sparsity constrain is believed to provide a new signal separation space which can alleviate some of the limitations of SVT in case of strong frequency and eigen spectral overlap. We show, through simulations, that the proposed method captures the tissue rank automatically and significantly penalizes the residual noise which does not fit in any of the two structured sup-spaces (low rank or sparse), hence providing significant improvement over SVT clutter removal under different tissue velocities and noise levels.

2. THEORY

Suppose $\mathcal{X} \in \mathbb{R}^{M\times N\times K}$ represents an ensemble of high frame rate ultrasound raw data where M and N are the number of samples in the axial (vertical) and lateral (horizontal) directions of an imaging frame respectively and K is the number of frames in the ensemble. By stacking mode-1 fibers of tensor $\mathcal{X}$, a 2-D spatial-temporal matrix $\mathbf{C} \in \mathbb{R}^{(M\times N)\times K}$, also known as Casorati matrix, can be formed. Echo data are assumed to be a mixture of strong tissue backscatter plus weak blood echoes and an additive noise component originating mostly from the electronic circuits. Hence $\mathbf{C}$ can be written as

$$\mathbf{C} = \mathbf{T} + \mathbf{B} + \mathbf{N} \tag{1}$$

where $\mathbf{T}$, $\mathbf{B}$ and $\mathbf{N}$ represent tissue, blood and noise components respectively. The task is to find an algorithm to separate blood echoes from the two other signals (i.e. tissue clutter and noise). When using high frame rate imaging, tissue motion can be assumed as a coherent process which results in a low rank matrix $\mathbf{T}$, using the mentioned data rearrangement method. Motions of the red blood cells in vessels and highly perfused areas, on the other hand, appear as processes with low degree of coherence and non-zero Doppler shift. Hence, $\mathbf{B}$, is not a low rank matrix in general. Additionally, blood vessels' spatial presence is much sparser than tissue components in each imaging frame. Hence, $\mathbf{B}$ can be assumed to be spatially sparse (sparse columns). This alone might suffice to provide incoherence requirement for the low rank plus sparse model indicated in [10] and used in [9]. However, signals across an ensemble of frames can cause rapid temporal fluctuations which might not be well represented as sparse signals in the time domain. Hence, it is appropriate to search for a transform domain that can provide a better sparse representation along the rows of $\mathbf{B}$ as well. The temporal Fourier transform can serve as a good candidate as Doppler shifts can be compactly represented by few spectral samples near the dominant Doppler peak. The noise component, $\mathbf{N}$, is neither low rank nor sparse, hence a low rank plus sparse framework is expected to significantly reject noise as solution approaches the optimal value. Hence, we formulate the low rank plus sparse clutter plus noise removal algorithm as the following

$$\min_{\mathbf{T}+\mathbf{B}=\mathbf{C}} rank(\mathbf{T}) + \boldsymbol{\lambda}\|\mathcal{F}\mathbf{B}\|_0 \tag{2}$$

where $\|\mathcal{F}\mathbf{B}\|_0$ is the number of non-zero elements of $\mathcal{F}\mathbf{B}$. The problem in (2) is non-convex and NP-hard [11]. Alternatively, a convex minimization surrogate with tractable complexity can be defined as

$$\min_{\mathbf{T}+\mathbf{B}=\mathbf{C}} \|\mathbf{T}\|_* + \lambda\|\mathcal{F}\mathbf{B}\|_1 \tag{3}$$

where λ is a tuning parameter, $\|\mathrm{T}\|_* = \sum_i \sigma_i(\mathbf{T})$ is the nuclear norm of $\mathbf{T}$ where σ_i is the i^{th} singular value and $\|\mathcal{F}\mathbf{B}\|_1 = \sum_{\mathrm{ij}}|(\mathcal{F}\mathbf{B})_{\mathrm{ij}}|$ denotes the l_1 norm of the $\mathbf{B}$ in a transformed domain (e.g. Fourier domain).

The constrained optimization in (3) can be cast as an unconstrained problem using regularization coefficients as

$$\min \ \frac{1}{2}\|\mathbf{C} - (\mathbf{T}+\mathbf{B})\|_2^2 + \lambda_t\|\mathbf{T}\|_* + \lambda_b\|\mathcal{F}\mathbf{B}\|_1 \tag{4}$$

where λ_t and λ_b create a balance between L+S regularization and data consistency. The problem in (4) can be solved using a two-step alternating minimization approach by solving one sub-problem at a time similar to [12]. In one step, a singular value soft thresholding recovers the best low rank approximation of $\mathbf{C}$ as $\mathbf{T}^*$. This estimate is then used to recover a sparse residue by element-wise soft thresholding of $(\mathbf{C} - \mathbf{T}^*)$. This process is summarized in Algorithm 1. A power Doppler image can be formed by rearranging matrix $\mathbf{B}$ based on the original spatial-temporal coordinate to from $\mathcal{X}_b \in \mathbb{R}^{M\times N\times K}$ and calculating the signal power at each pixel as

$$\mathbf{P}(m,n) = \frac{1}{K}\sum_{k=1}^{K}|\mathcal{X}_b(m,n,k)|^2 \tag{5}$$

Algorithm 1: alternating minimization for low rank plus sparse problem in (4)

Input: Casorati echo data matrix $\mathbf{C}$, $\boldsymbol{\lambda_t}$, $\boldsymbol{\lambda_b}$ and sparsity promoting transform $\mathcal{F}$

Initialize: $\mathbf{C_0} = \mathbf{C}$, $\mathbf{B_0} = \mathbf{0}$, convergence rule

While (convergence rule not met)

$\mathbf{T}_{\boldsymbol{k}} = \boldsymbol{SVT}_{\lambda_t}(\mathbf{C}_{\boldsymbol{k-1}} - \mathbf{B}_{\boldsymbol{k-1}})$ **//** $\boldsymbol{SVT}_{\lambda_t}$*: low rank soft singular value thresholding*

$\mathbf{B}_{\boldsymbol{k}} = \mathcal{F}^{-1}\boldsymbol{THR}_{\lambda_b}(\mathcal{F}(\mathbf{C}_{\boldsymbol{k-1}} - \mathbf{T}_{\boldsymbol{k}}))$ **//** $\boldsymbol{THR}_{\lambda_b}$*: sparsity soft thresholding*

$\mathbf{C}_{\boldsymbol{k}} = \mathbf{T}_{\boldsymbol{k}} + \mathbf{B}_{\boldsymbol{k}}$

end

Output: $\begin{cases}\mathbf{T} \leftarrow \mathbf{T}_{\boldsymbol{k}} \\ \mathbf{B} \leftarrow \mathbf{B}_{\boldsymbol{k}}\end{cases}$

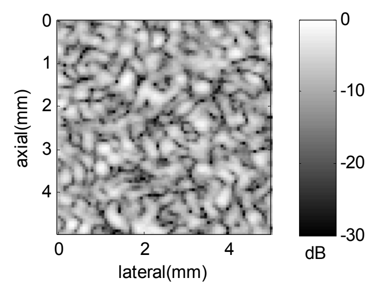

Fig. 1: B-mode image obtained from the first frame of the simulated IQ data.

3. SIMULATIONS

To evaluate the performance of proposed method in terms of power Doppler images and provide a comparison with those of SVD a simulation study was performed. We employed a point spread function (PSF) approach for creating simulation data. In this method, the PSF of the imaging system is derived as a two-dimensional kernel. The medium is then modeled as a collection of ultrasound scatterers with random amplitudes which represent tissue/blood reflectivity coefficients. We adopted the method in [9] for both PSF calculation and scatterer creation and motion. The PSF was derived for a multi-angle compounding plane wave imaging system with maximum steering angle of 7° operating at 6MHz. Tissue and red blood cells were then modeled as a collection of 50000 scatterers uniformly distributed over an area of $5mm^2$. A vertical vessel with diameter of $500\mu m$ was modelled at the center of the image. Tissue scatterers were assumed to create 5 times stronger echoes than blood scatterers. To simulate combined tissue-blood motions an stochastic model which accounts for both translational and

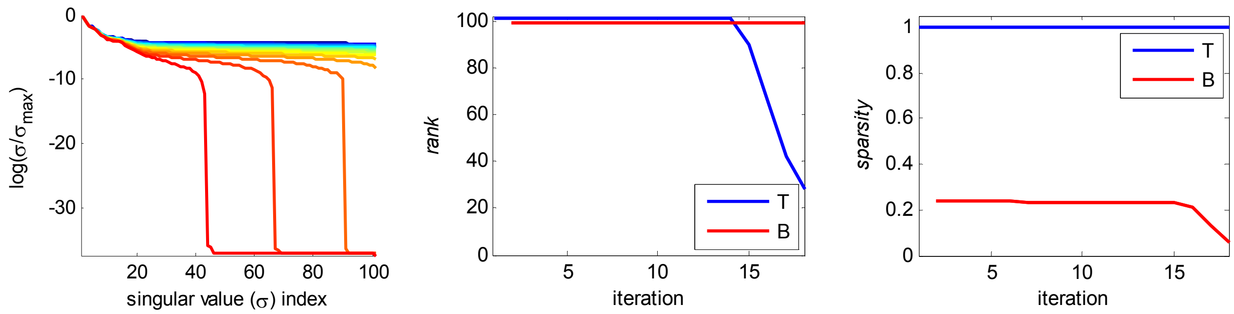

(a) (b) (c)

Fig. 2: (a) singular energy decay of the low rank part **T** as a function of iterations (deep blue: first iteration, deep red: last iteration) (b) rank of the low rank part **T** (blue) and sparse part **B** (red) as a function of iterations and (c) sparsity of the low rank part **T** (blue) and sparse part **B** (red) as a function of iterations. In all cases, tissue velocity=5mm/s, SNR=20dB.

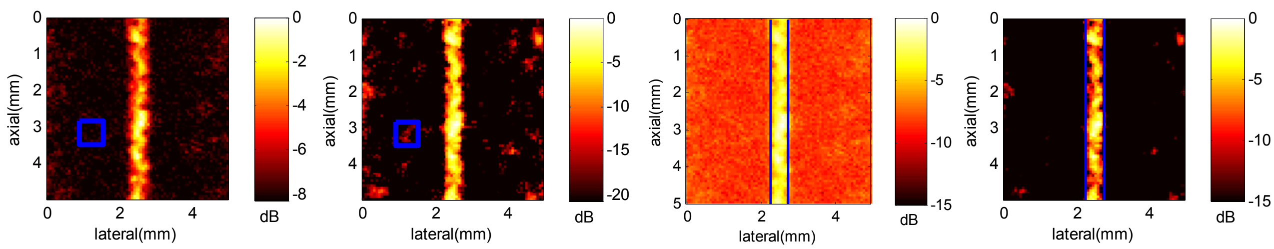

(a) (b) (c) (d)

Fig. 3: (a) power Doppler image obtained by SVD shown at the best dynamic range. Minimum power was obtained from a region outside vessel (blue square) (b) power Doppler image obtained by L+S shown at the best dynamic range (c) power Doppler image obtained by SVD at 15dB dynamic range with the vessel walls overlaid as vertical blue lines (d) power Doppler image obtained by L+S at 15dB dynamic range with the vessel walls overlaid as vertical blue lines. In all cases, tissue velocity=5mm/s, SNR=20dB.

shearing motions was adopted based on [9]. The mean tissue velocity was $5\,mm/s$ and maximum shearing was 1%. Maximum blood velocity was $10\,mm/s$ with a laminar flow such that mean blood velocity was half of the maximum. A total of 101 frames of in-phase and quadrature (IQ) data were created at a frame rate of 1000 frames per second (i.e. $\sim 100ms$). To analyze the effect of tissue motion, simulations were repeated for tissue velocities of 5mm/s, 10mm/s and 15mm/s. Additionally, different levels of additive white complex Gaussian noise were considered to create three SNR values of 26dB, 20dB and 14dB. Both SVD and the proposed low rank plus sparse (L+S) method were applied to the simulated data. For SVD, an optimal clutter rank of 10 was chosen empirically based on the maximum clutter speckle rejection and best vessel visibility in the power Doppler image. The L+S parameters λ_t and λ_b were also chosen empirically as $8 \times 10^{-4}\sigma_1$ (σ_1: largest singular values of $\mathbf{T}$) and $1.58 \times 10^{-5}\|\mathbf{C_0}\|_2$ respectively. The number of iterations was used as the stopping criteria and it was set to 18. In the following, sparsity of matrix $\mathbf{X} \in \mathbb{R}^{M \times N}$ is defined as $\|\mathbf{X}\|_0/(MN)$ which is the ratio of the number of non-zero elements to the total number of elements.

4. RESULTS

Fig. 1 shows the B-mode image obtained from the IQ data in the first frame of the simulated data ensemble. As it can be seen, the blood vessel cannot be identified at the center of the image due to strong tissue clutter. Fig. 2(a) shows the singular value behavior of the low rank part **T** as a function of iteration index. The monotonic decay in the normalized singular values is indicative of low rank absorption by **T** and overall convergence of the two-step Algorithm 1. This can be further verified in Fig. 2(b) and Fig. 2(c) where rank and sparsity of the low rank matrices **T** and **B** are presented respectively. As it can be seen, while **T** shows a monotonic rank decay, **B** maintains a high rank value. On the other hand, while **T** is preserved as a dense matrix, **B** becomes sparser as the algorithm progresses. It should be noted that due to soft thresholding, no significant change is observed in both the rank of **T** and sparsity of **B** in the first few iterations. Fig. 3 (a) and Fig. 3 (b) show the power Doppler images resulted from SVD and L+S respectively. For best visualization, the average power Doppler of the residual clutter+noise from an area outside the vessel region (blue square in Fig 3) was used as the minimum value for the dynamic range in each method. While both SVD and L+S have provided acceptable clutter suppression, L+S shows superior background removal compared to SVD without affecting the vessel structure. To better appreciate this, Fig. 3(c) and Fig. 3(d) present power Doppler images at the same dynamic range (15dB) for both methods. While both methods have successfully removed the clutter signal such that the resulting vessel images corroborate with the geometry used in the simulation (vertical blue lines), significant background noise is observed in the SVD image. To further analyze the processing gain obtained by L+S over SVD, the average power Doppler over all depths was obtained and is depicted in Fig. 4 and Fig. 5 for different SNRs and tissue velocities respectively. L+S provided a minimum of 14dB, 6dB and 2dB improvement over SVD at SNR=26dB, 20dB and 14dB respectively. In terms of robustness to tissue motion, L+S provided a minimum of 2.5dB, 3dB and 12dB improvement over SVD for tissue velocities of 20mm/s, 10mm/s and 5mm/s respectively. Finally, Fig. 6 depicts the estimated Doppler spectrum at a point inside vessel using SVD (blue) and L+S (red) methods where the latter has resulted in significant reduction of the spurious spectral components which are mostly due to in-band noise (SNR=20dB, tissue velocity=5mm/s). The selective suppression of the in-band noise justifies the background removal gain obtained by the L+S method compared to SVD.

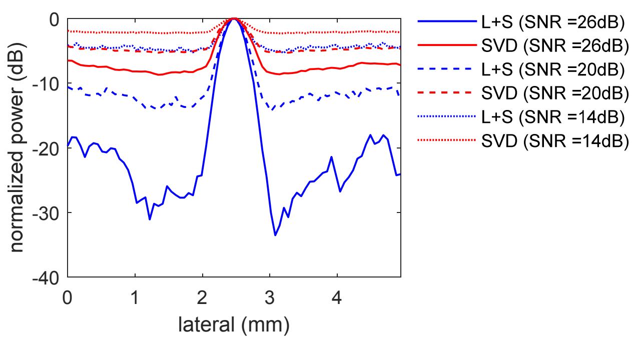

Fig. 4: lateral distribution of the power Doppler averaged over all depths using SVD and L+S at different SNR values.

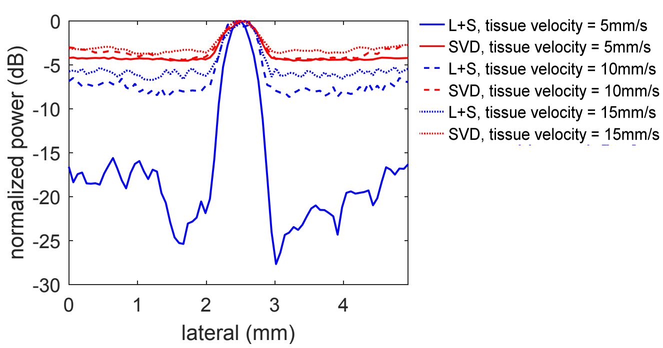

Fig. 5: lateral distribution of the power Doppler averaged over all depths using SVD and L+S for different tissue velocities.

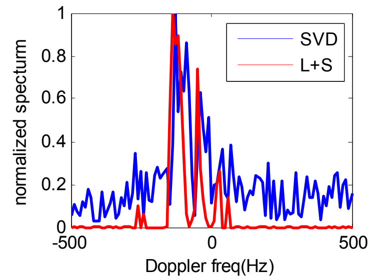

Fig. 6: Doppler spectrum estimated at a point inside vessel area using SVD (blue) and L+S (red).

5. CONCLUSION

In this paper, a low rank plus sparse model for concurrent clutter and noise removal from ultrasound Doppler ensembles was presented. A two-step alternating minimization algorithm based on soft singular value thresholding and soft element-wise thresholding in temporal frequency domain was proposed. A simulation model which integrates both imaging system features and realistic tissue motions and deformations was employed. The latter was a significant improvement over similar simulation studies which only consider tissue translational motion, hence ignoring possible pulse compressions due to shearing deformations which are inventible in imaging *in vivo*. Our simulation results showed that L+S can favorably absorb tissue related motions in a low rank component while blood related motions were modeled as a near full rank matrix with both spatial and (frequency) spectral sparsity. The unstructured noise was significantly penalized through this process, leading to superb blood-background separation. It was shown that L+S provides better clutter removal and noise suppression under different tissue motion levels and noise powers when compared to SVD. Future studies will include finding selection criteria for optimal values of λ_t and λ_b under different tissue motions and noise conditions and testing the proposed method on *in vivo* data.

6. ACKNOWLEDGEMENT

This work was supported in part by the U.S. National Institutes of Health grant R01CA168575. We would like to thank the authors in [9], for their assistance with producing the simulation data.

12. REFERENCES

[1] C. Demené, T. Deffieux, M. Pernot, B. F. Osmanski, V. Biran, J. L. Gennisson, L. A. Sieu, A. Bergel, S. Franqui, J. M. Correas, I. Cohen, O. Baud, and M. Tanter, "Spatiotemporal Clutter Filtering of Ultrafast Ultrasound Data Highly Increases Doppler and fUltrasound Sensitivity," *IEEE Transactions on Medical Imaging,* vol. 34, pp. 2271-2285, 2015.

[2] P. Song, A. Manduca, J. D. Trzasko, and S. Chen, "Ultrasound Small Vessel Imaging With Block-Wise Adaptive Local Clutter Filtering," *IEEE Transactions on Medical Imaging,* vol. 36, pp. 251-262, 2017.

[3] M. Bayat, M. Fatemi, and A. Alizad, "Background-free visualization of microvasculature networks," in *2017 IEEE International Ultrasonics Symposium (IUS)*, 2017, pp. 1-1.

[4] L. A. F. Ledoux, P. J. Brands, and A. P. G. Hoeks, "Reduction of the Clutter Component in Doppler Ultrasound Signals Based on Singular Value Decomposition: A Simulation Study," *Ultrasonic Imaging,* vol. 19, pp. 1-18, 1997.

[5] F. W. Mauldin, D. Lin, and J. A. Hossack, "he Singular Value Filter: A General Filter Design Strategy for PCA-Based Signal Separation in Medical Ultrasound Imaging," *IEEE Transactions on Medical Imaging,* vol. 30, pp. 1951-1964, 2011.

[6] A. C. H. Yu and L. Lovstakken, "Eigen-based clutter filter design for ultrasound color flow imaging: a review," *IEEE Transactions on Ultrasonics, Ferroelectrics, and Frequency Control,* vol. 57, pp. 1096-1111, 2010.

[7] D. E. Kruse and K. W. Ferrara, "A new high resolution color flow system using an eigendecomposition-based adaptive filter for clutter rejection," *IEEE Transactions on Ultrasonics, Ferroelectrics, and Frequency Control,* vol. 49, pp. 1739-1754, 2002.

[8] V. A. Marčenko and L. A. Pastur, "Distribution of Eigenvalues for Some Sets of Random Matrices," *Mathematics of the USSR-Sbornik,* vol. 1, p. 457, 1967.

[9] G. S. Alberti, H. Ammari, F. Romero, and T. Wintz, "Mathematical Analysis of Ultrafast Ultrasound Imaging," *SIAM Journal on Applied Mathematics,* vol. 77, pp. 1-25, 2017.

[10] E. J. Candes, X. Li, Y. Ma, and J. Wright, "Robust principal component analysis?," *J. ACM,* vol. 58, pp. 1-37, 2011.

[11] A. L. Chistov and D. Y. Grigor'ev, "Complexity of quantifier elimination in the theory of algebraically closed fields," in *Mathematical Foundations of Computer Science 1984: Proceedings, 11th Symposium Praha, Czechoslovakia September 3–7, 1984*, M. P. Chytil and V. Koubek, Eds., ed Berlin, Heidelberg: Springer Berlin Heidelberg, 1984, pp. 17-31.

[12] R. Otazo, E. Candès, and D. K. Sodickson, "Low-rank plus sparse matrix decomposition for accelerated dynamic MRI with separation of background and dynamic components," *Magnetic Resonance in Medicine,* vol. 73, pp. 1125-1136, 2015.